Université de Paris | université angers | UNIVERSITÀ DI PAVIA | UNIVERSITY OF PATRAS

NANOMED

Erasmus Mundus Joint Master Degree (EMJMD) Nanomedicine for Drug Delivery (NANOMED)

6 months traineeship report

Years 2020/2022

(This report is confidential)

EVALUATION OF THE PHYSICOCHEMICAL PROPERTIES AND THE HEAT-TRIGGERED PAYLOAD RELEASE FROM THERMOSENSITIVE CATIONIC LIPOSOMES FORMULATED WITH A NOVEL LIPID

Date of defense: 13th of July 2022

Thales do Valle Moreira

Supervisor: Prof. Dr. med. Lars H. Lindner

Cosupervisor: Dr. rer. nat. Matteo Petrini

Date: 28/06/2022

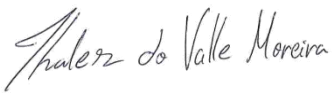
Signatures

Klinikum der Ludwig-Maximilian-Universität München & Thermosome GmbH, Munich, Germany.

'No-plagiarism commitment statement'

By this statement, I certify that I acknowledge plagiarism of a document, in part or as a whole, violates copyrights and constitutes an outright fraud. I hereby certify that this report is my own work, based on my personal study and/or research and that I have acknowledged all material and sources used in its preparation, whether they be books, articles, reports, lecture notes, and any other kind of document, electronic or personal communication. I also certify that this report has not previously been submitted for assessment in any other unit, except where specific permission has been granted from all unit coordinators involved, or at any other time in this unit, and that I have not copied in part or whole or otherwise plagiarized the work of other students and/or persons.

Name: Thales do Valle Moreira **Date**: 28/06/2022

Signature 

PRELIMINARY DISCLAIMER

This document is strictly confidential. Some of the references for and findings of this work are yet unpublished material. Intellectual property belongs to Klinikum der Universität München, which itself has legal obligations towards Thermosome GmbH regarding such titles, and/or Thermosome GmbH. Any use of it, either partially or fully, infringes the signed Non-Disclosure Agreement.

ABSTRACT

Background: Heat-triggered local drug release rose as a promising strategy to treat localized diseases while reducing systemic off-target side effects. Thermosensitive liposomes (TSL) successfully exploit this targeting strategy, especially against solid tumors [1,2]. TSLs with negatively charged diglycerol-headed lipid have been described to allow sharp control drug release [3] and prolong circulation half-life ($T_{½}$) without using polyethyleneglycol (PEG), avoiding related concerns [4]. Furthermore, a positive surface charge helps target cancerous cells and associated vasculatures [5] overexpressing negatively charged membrane-proteins and aberrant glycocalyx [6]. **Objectives:** the formulation of a novel diglycerol-functionalized ionizable cationic lipid (NICL) into cationic TSL (CTSL) was investigated. Here, the formulation screening of NICL-based CTSLs and their physicochemical characterization are thoroughly reported. **Results:** regardless of vesicle size (obtained by extrusion), zeta-potential (ZP) correlated with NICL mol%, resembling previously reported anionic TSL (ATSL) [4,5,7]. At pH 7.2, stable CTSL loaded with carboxyfluorescein (an anionic molecular marker; CF) could be formed with 10, 20, and 30 mol% NICL. Diluting the CTSL in buffers at different pHs immediately affected the ZP but not liposomal size, until the isoelectric points (pI) were reached (~pH 9), triggering aggregation. CF heat-triggered release from CTSL was affected by the liposomal size and NICL mol%. Smaller liposomes with less NICL showed higher release rates. It correlated with the clearer phase-transition temperature (T_m) by differential scanning calorimetry (DSC). **Conclusions:** NICL can be formulated into CTSL similarly to previously published TSLs [4,5,7] with heat-responsiveness confirmed for a range of different formulations, the best at 10 mol% NICL and 50 nm. NICL-CTSLs behave as polyelectrolytes in aqueous media, with pKa ranging from 7.6 to 8.20 here.

KEYWORDS

Ionizable Cationic lipid; Diglycerol; Thermosensitive Liposomes; Formulation.

TABLE OF CONTENTS

1. INTRODUCTION 1

2. MATERIALS AND METHODS 3

2.1. Chemicals 3

2.2. Liposomal formulations 3

2.3. Characterization of the liposomes 3

2.4. Temperature-dependent CF-release and liposomal-CF content 4

2.5. Time-dependent CF-release 4

2.6. Zeta-Titration 4

2.7. Live-cell fluorescence microscopy 5

2.8. Data treatment and statistics 5

3. RESULTS 5

3.1. NICL can be formulated into TSL depending on mol% included 5

3.2. CF-release from NICL-CTSL is temperature- and time-dependent. 8

3.3. Increasing NICL mol% makes T_m and drug-release less defined. 10

3.4. In aqueous systems, NICL-CTSLs behave as polyelectrolyte. 10

3.5. NICL-CTSL bind to tumor cells *in vitro* better than ATSL. 12

4. DISCUSSION 14

5. CONCLUSIONS AND PERSPECTIVES 15

6. ACKNOWLEDGMENTS 16

8. SUPPLEMENTARY INFORMATION 20

1. INTRODUCTION

Liposomes are supramolecular vesicular structures formed upon the self-assembly of lipids and lipidoids [2]^{p121}. They raised great interest in drug delivery since first described in 1964 by Alec Bangham [2]$^{pp524-528}$. Three decades later, Doxil®/Caelyx® (doxorubicin [DOX] HCl liposome injection, Johnson & Johnson, New Brunswick, NJ, USA) became the first approved nano- and liposomal drug. It was in 1995 by the Food and Drug Authority and in 1996 by the European Medicines Agency. To date, at least 14 unique liposomal formulations (excluded generics and lipid complexes like Onpattro®, Abelcet®, and Amphotec®) made it into the market after showing improved control of targeting, release, and degradation of the payload, as well as biocompatibility and safety [8].

Concerning clinical examples, however, targeting so far relied mainly on the passive accumulation in inflamed and poorly drained tumor tissues that often display leaky aberrant neovasculature. To benefit from the enhanced permeation and retention (EPR) effect, formulations must circulate long enough to accumulate in the diseased area. Coating with polyethylene glycol (PEG), thus rendering them *stealth*, is a widely explored strategy for improving circulation half-life ($T_{½}$). The hydration of the PEG chains creates steric hindrance, reducing protein adsorption. It modulates protein corona formation, then opsonization, and ultimately delays the recognition by the mononuclear phagocytic system (MPS) and clearance [9]. Still, PEGylation most often only significantly improved drug safety, but seldom its efficacy [4,10].

Moreover, the EPR effect has been put into question and its clinical relevance is under debate due to the strong heterogeneity of patients and poor level of experimental data showing effectiveness [11]. Hence the growing interest in active targeting and stimuli-responsive systems as alternatives [2]$^{pp589-593}$.

Another interest in PEG-free formulations concerns avoiding PEG-induced complement activation-related pseudoallergy (CARPA), a likely serious hypersensitive reaction [9]. Moreover, pharmacokinetics on subsequent doses might be negatively affected by anti-PEG antibodies. These can be formed at the first liposome administration – being detectable even in liposome-naïve patients, likely due to routine exposure to PEG-containing products – and it can lead to the accelerated blood clearance (ABC) phenomenon [4].

First reported by Yatvin et al in 1987, thermosensitive liposomes (TSL) release their payload when heated above their melting (or solid gel to liquid disordered) phase-transition temperature (T_m). Synergistically, local mild hyperthermia (41-43 °C; HT) can also contribute to tenderizing the tumor, increasing blood flow, hence enhancing the access of cellular and humoral immune factors as well as drugs [12]. This is notably useful against localized tumors like soft tissue sarcoma [1]. Several things can affect TSL heat-triggered drug release, notably vesicle size. Smaller ones release their content better [13].

Conceived in 1995 and invented in 1996 [2]$^{pp528-530}$, a TSL formulation by Needham et al first attempted clinical trials in 2005 [14]. It employed lysolipids (LTSL), derivatives lacking one acyl tail [1,14,15], which allowed for ultra-fast drug release at low temperatures. Later called ThermoDox®, this formulation proprietary to Celsion Corporation (Columbia, MD, USA) was tested in combination

with radiofrequency ablation [14]. It failed in a second Phase III clinical trial in 2021 despite its noteworthy DOX burst release. Still, its clinical development taught a great deal about heating techniques and protocols, [14] as well as formulation design [1,8,14].

Thermosome GmbH (Planegg, Germany) has been developing a novel TSL platform based on oligo-glycerol headgroups for anticancer treatments [1,3–5,7,14,16]. Fine-tuning of the T_m and the sharp control of intravascular drug release were shown with a PEG- and cholesterol-free anionic TSL (ATSL) based on 1,2-dipalmitoyl-*sn*-glycero-3-phosphoryldiglycerol ($DPPG_2$) [3]. A video summarizing the dual-targeting technology is available on the website of the company [17].

Compared to conventional liposomal-DOX (Caelyx®) and LTSL-DOX, a $DPPG_2$-based DOX-loaded formulation plus mild HT notably improved survival in a rat soft tissue sarcoma model. Importantly, $DPPG_2$-TSL-DOX performed overall better than free-DOX in locally advanced spontaneous feline sarcoma in a comparative oncological study combined with localized-HT in the neoadjuvant setting [3]. In a pig model, the intravenous (IV) administration of this formulation plus mild HT showed increased DOX delivery with higher bladder biodistribution than IV or intravesical free-DOX, paving a rationale for muscle-invasive bladder cancer treatment [16]. At 30 mol%, $DPPG_2$-based TSL displayed increased circulation $T_{½}$ and reduced immunogenicity (vs. TSL with lower $DPPG_2$ content). Recently, a distinguished protein corona profile with a high abundance of apolipoprotein E (ApoE) was reported. It was associated with positive modulation of complement activation, biodistribution, and clearance [4].

Despite being cleared faster due to more intense opsonization, cationic nanoparticles showed better targeting of tumor cells. These overexpress negatively charged membrane proteins, rendering their cell surfaces distinguishably negatively charged [1,5,18]. The homing of cationic TSL (CTSL) to tumors and their associated vasculature followed by HT-induced intracellular DOX nanoburst was reported [18]. More recently, $DPPG_2$-based CTSLs showed similar features. In comparison to a PEG-CTSL, tumor cell-targeting was 3.4 times higher in fluorescence-activated cell sorting (FACS), half-maximal inhibitory concentration (IC_{50}) was 3.5-fold lower, and live-cell fluorescence microscopy showed superior internalization and DOX delivery after HT. Despite the better liposome-cell interactions of $DPPG_2$-CTSL, the pharmacokinetics and biodistribution *in vivo* were suboptimal, with faster clearance highlighted by a $T_{½}$ 8.1-times shorter than PEG-TSL [5].

From these findings, it was hypothesized that the diglycerol head group could balance the fast clearance of cationic nanoparticles while keeping the tumor-targeting feature while avoiding the presented PEG- and lysolipid-related issues. Therefore, here it is reported the formulation screening of TSL bearing a novel ionizable cationic lipid (NICL). Carboxyfluorescein (CF)-loaded ionizable CTSLs were prepared with different membrane extrusion sizes to thoroughly assess the effect on lipid bilayer, size-distribution, zeta-potential (ZP), and heat-responsiveness. Furthermore, a ZP-titration within the pH range from 2 to 11 was performed to clarify the effect of pH over surface charge and assess the pKa of the different NICL-CTSLs.

2. Materials and Methods

2.1. Chemicals

Thermosome GmbH (Planegg, Germany) provided $DPPG_2$ and NICL. 1,2-dipalmitoyl-*sn*-glycero-3-phosphocholine (DPPC) and 1,2-distearoyl-*sn*-glycero-3-phosphocholine (DSPC) were acquired from Corden Pharma Switzerland LLC (Liestal, Switzerland). 1,2-dipalmitoyl-*sn*-glycero-3-phosphoethanolamine-N-(7-nitro-2-1,3 benzoxadiazol-4-yl) (NBD-PE) was purchased from Avanti Polar Lipids (Alabaster, AL, USA). Fetal calf serum (FCS) and CF free acid were bought from Sigma Aldrich (Darmstadt, Germany). Höchst 33342 and Lysotracker Red99 from ThermoFisher Scientific (Waltham, MA, USA).

All other chemicals were either from Sigma Aldrich GmbH (München, Germany) or Carl Roth GmbH (Karlsruhe, Germany). Unless stated, all the buffers and solutions mentioned in the study were prepared with ultrapurified deionized water from an ultrapure water system Milli Q Advantage from Merck Millipore (Darmstadt, Germany).

2.2. Liposomal formulations

As previously reported, but starting from lipid stock solutions prepared in chloroform:methanol (9:1 vol/vol), lipid films composed by DPPC/DSPC/NICL (80-X:20:X, X=5-75 mol/mol, coded in **Table 1**) were obtained, then hydrated and manually extruded at 60°C. ATSL with 30 mol% $DPPG_2$ was prepared as described elsewhere [3–5,19,20]. Neutral TSLs extruded at 50 nm (0TSL-50) were prepared using DPPC/DSPC with an 8:2 molar ratio. 0.3 mol% of NBD-PE were included in the lipid bilayer of TSLs submitted to fluorescence microscopy.

Lipid films were stored at room temperature under vacuum until being hydrated with 100 mM CF pH 7.2 (or HBS pH 7.4 for NBD-PE-labelled liposomes without CF) at 60 °C under agitation during 10 min. Then, the colloidal suspension was extruded (Avestin, Ottawa, Canada) 17 times through 200, 100, and 50 nm polycarbonate filters (Cytiva, MA, USA; and Avestin, Ottawa, Canada) at 60 °C.

Non-encapsulated CF was removed while changing the extraliposomal media by size exclusion chromatography (SEC) employing Sephadex G50 (APBiotech, Uppsala, Sweden) equilibrated with HBS pH 7.4.

Within this document, NICL-based formulations are coded as NICL together with the mol% of NICL included in the film, dash the size-cutoff of the filter used for its extrusion (e.g., 5 mol% NICL extruded through 100 nm filters is coded NICL5-100, listed in **Table 1**).

2.3. Characterization of the liposomes

Size (hydrodynamic diameter as Z-average), polydispersity index (PDI), and ZP were measured by dynamic lighting light scattering (DLS) with a Zeta Sizer Nano ZS (Malvern Instruments, Worcestershire, UK). Samples were diluted 50-times in sterile filtrated NaCl 0.9 % m/v (saline). Size and PDI were simultaneously determined in disposable plastic cuvettes while three ZP measurements separated by 30 s were made per sample in a disposable folded capillary cuvette.

Osmolality and pH of formulations and buffers were measured respectively with an Osmometer (VAPRO 5600 Vapor Pressure, Wescor. Inc, Logan, USA) and with a pH meter (Inolab pH 720, WTW, Weilheim, Germany). The 100 mM CF solution at pH 7.2 had an osmolality of 220 mOsm/kg, while the saline used on DLS has 287 mOsm/kg.

Freshly prepared formulations were submitted to differential scanning calorimetry

(DSC, Mettler Toledo DSC 821e, Giessen, Germany) after being concentrated to 35-60 mM via centrifugal filtration (Amicon filters 30K, Merck-Millipore, Darmstadt, Germany). T_m was determined as the peak value of the endothermal event on the heating phase of the thermogram acquired from 20 to 60 °C with a step of 1 °C/min.

Using reference standards (except for NICL), lipid contents were confirmed and degradation products were quantified by high-performance liquid chromatography (HPLC, Scientific Dionex™ Ultimate, 3000) employing a methanol-based gradient and a charged aerosol detector (CAD, Corona Veo, ThermoFisher, Waltham, MA, USA), before and after purification, when applicable. Due to the absence of an available commercial standard, NICL was estimated from peak area %.

2.4.Temperature-dependent CF-release and liposomal-CF content

As previously [19], CF-loaded TSLs were first diluted in 0.9% saline and then either in 0.9% saline or FCS. Aliquots (technical duplicates) of each liposomal dilution were heated (Thermoshaker, Eppendorf AG, Hamburg, Germany) under shaking (750 rpm) for either 5 (room temperature, RT, and 37 to 45 °C) or 60 (37 and 42 °C) min before being finally diluted in refrigerated (4 °C) tris-buffered saline (TBS), stopping the CF-release. Fluorescence intensity at each temperature ($I_{T°C}$) was measured (Cary Eclipse, Varian Inc., Palo Alto, USA; ex/em 493/513 nm, 625 V, 2 s, 1 cm) and compared with the total liposomal-CF content or 100% CF-release (I_{Triton}). The latter was observed in samples diluted similarly with the addition of 10% Triton X-100 v/v and incubating the suspension at 45 °C, under 750 rpm, for 15 min. The CF release was calculated as:

$$Released\ CF = \frac{I_{T\,°C} - I_{RT}}{I_{Triton} - I_{RT}} \times 100$$

The CF content (C_{CF}) is obtained by interpolating I_{Triton} in a CF standard curve (0.033 to 0.976 µM). Encapsulation efficiency (EE) is given by the final-over-the-initial ratio of the CF- over the lipid-concentrations ratio:

$$EE = \frac{(C_{CF}/C_L)_{Final}}{(C_{CF}/C_L)_{initial}} \times 100$$

2.5.Time-dependent CF-release

As previously published [19], CF-loaded formulations were diluted in HBS pH 7.4 (technical duplicates). For 100% CF-release (I_{Triton}), equal parts of the sample and 10% Triton X-100 v/v were stirred together (750 rpm) at 45 °C for 15 min, before diluting it further in HBS pH 7.4 (single sample). All samples were finally diluted in pre-warmed FBS and fluorescence intensities were recorded 17 times over 300 s at 30 and 37-43 °C. CF release was calculated as in 2.4 and fit with an exponential one-phase association.

2.6.Zeta-Titration

Size, PDI, and ZP were measured as in 2.3., but in a sterile filtrated buffer composed of 20 mM Na_3PO_4, 25 mM monosodium citrate, 20 mM NH_4AcO, and enough NaCl to reach 290 mOsm/kg after adjusting the pH from 2 to 11 with HCl and NaOH 1, 2, and 4 N. The buffers' osmolality was checked before and after setting the pH for adjusting the osmolality with NaCl. Then, based on the work by Carrasco et al [21], pKa values of CTSL formulations were estimated after fitting pH and ZP values to the extended Henderson-Hasselbach (eHH) equation:

$$ZP = ZP_{max} - \frac{ZP_{max} - ZP_{min}}{1 + 10^{(pH-pKa)/n}}$$

Table 1. *Lipid composition of the screened formulations, their codes, and observations on their behavior during TSL preparation. The ones in bold formed monodisperse liposomal suspension, hence the comments on their colloidal stability when stored overnight in the fridge (4 °C). The number of * indicates how comparatively faster the CTSL sedimentation is observed.*

Lipid film composition (mol%)				**Extrusion filter pore diameter (nm)**		
Code	**DPPC**	**DSPC**	**NICL**	**200**	**100**	**50**
NICL5	75	20	**5**	Polydisperse	Monodisperse*****	Monodisperse****
NICL10	70	20	**10**	Polydisperse	Monodisperse****	Monodisperse***
NICL20	60	20	**20**	Monodisperse***	Monodisperse***	Monodisperse**
NICL30	50	20	**30**	Monodisperse**	Monodisperse**	Monodisperse*
NICL50	30	20	50	Ruled out	Gels on cooling	Gels on cooling
NICL75	5	20	75	Ruled out	Unable to extrude	Ruled out
NICL100	0	0	100	Does not hydrate with CF 100 mM pH 7.2 or HBS 7.4		

2.7. Live-cell fluorescence microscopy

Adherent mouse melanoma cells (B16 F10, ATCC, VA, USA) were cultured in Dulbecco's Modified Eagle Medium (DMEM, ATCC, VA, USA) supplemented with 10% supplemented fetal bovine serum (FBS, Superior, Sigma, Steinheim, Germany) and 1% penicillin-streptomycin (PenStrep, Sigma, Darmstadt, Germany). The incubator was set up (Binder, Tuttlingen, Germany) with a humidified atmosphere containing 95% air and 5% CO_2 at 37 °C. Cell handling was done under sterile conditions and the cell flasks were open only inside a laminar flow hood (Glaire BSB 4, ICN Flow, Eggenstein, Germany). Cell detachment was achieved by incubation with 0.25% Trypsin (Biochrom, Berlin, Germany) at 37°C for 2 minutes. Cell passages were performed when reached to 70-80% confluence (every 2-3 days).

25,000 cells were seeded in each well of a chambered coverslip (µ-Slide 8 well ibiTreat, Ibid, Germany) for the live-cell fluorescence microscopy experiments. 24 h after, the culture media was removed and replaced by 250 µL of 1 mM lipid samples. Past 30 min, 50 µL of 0.5 µM Lysotracker Red in FBS-free DMEM was added. The medium was removed 30 min later and, after washing the cells with FBS-free DMEM, 300 µL of Höchst 5 µg/mL in PBS were added. 5 min later, it was removed, and the cells were washed with PBS. A Leica wide-field microscope was used to observe the cells and the images were acquired with the Leica LAS X image software (Leica, Germany). Pictures were treated on ImageJ software version 1.8.0_172 afterward.

2.8. Data treatment and statistics

GraphPad Prism software version 9.3.1 (471) was used to plot the data into graphs. Unless stated otherwise, data are reported as the mean of three independent experiments ± standard error of the mean (SEM).

3. Results

3.1. NICL can be formulated into TSL depending on mol% included

Lipid films with different final NICL mol% were prepared to investigate NICL in terms of CTSL-forming excipient. The formulations with 5, 10, 20, and 30 mol% NICL met the quality criteria as hydration, extrusion, and

formation of a monodisperse distribution after purification were successful (**Table 1**). Given the trends across the first four formulations, 200 nm filters were early ruled out for being suboptimal. Moreover, these samples were tipping both the size and the PDI thresholds of a target product profile for injectable nanomedicines [2][pp107-113,120-124].

A summary of the composition analyses by HPLC-CAD (for the lipids) and fluorimetry (for CF) is given in **Figure 1**. Extrusion diameter did not significantly affect any of the outputs. However, the lipid content showed to decrease with increasing NICL mol%. In the same direction, although more subtly, the CF-content was also observed to decrease, not the EE, which was generally observed to be between 4.8 and 8.2 %. The CF content decrease might simply be interpreted as a mathematical compensation for the lower lipid content. The formulation yield tended to decrease with NICL mol%, but it does not seem to be affected by extrusion size.

The lipid content of DPPC and DSPC, respectively, varied mostly within 10 and 20% from the nominal values in the planned formulations. Except for 5 mol%, NICL values varied mostly within the 20% range. The absence of standard combined with the low intensity of CAD signal could help explain the overestimation for NICL5 (**Figure SI 1**).

To compare with another diglycerol-based TSL, a pre-established ATSL formulation (DPPC/DSPC/$DPPG_2$, 50:20:30) [3–5] was reproduced with only minimal variation in the used extrusion filter pore diameter. $DPPG_2$–based ATSLs lipid composition and content were consistent and reproducible, on top of being more precisely determined due to standard availability.

With 10, 20, and 30 mol%, NICL was able to form liposomes when mixed in the phosphocholine-based bilayer, with size/PDI depending on different factors (**Figure 2**). The diameter of the extrusion filter was identified as a critical process parameter, as suggested in **Table 1**. It directly affects the size and, consequently, the colloidal stability too.

After being extruded through 200 nm filters, samples with 5 and 10 mol% NICL

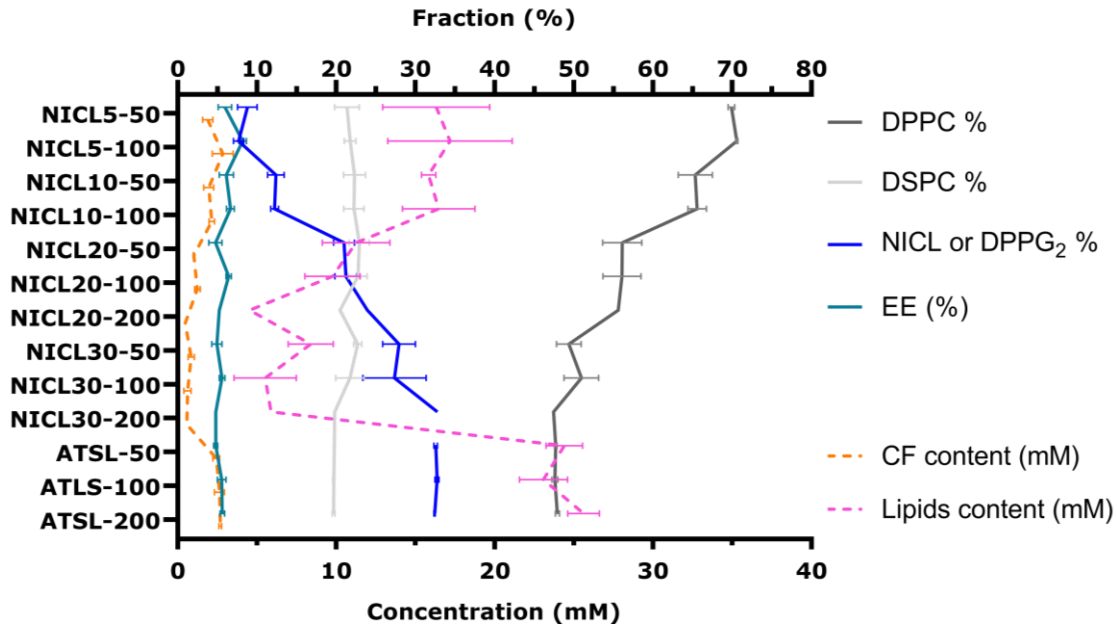


Figure 1. *Summary of HPLC-CAD and fluorimetric results: lipid composition and EE (solid lines, upper Y-axes) plus lipid and CF (dashed lines, lower Y-axis) contents for different formulations.*

quickly underwent aggregation, depicted on DLS by a multimodal distribution across the nano- and micrometer ranges or a unimodal distribution centered close to 1000 nm. A similar trend but much more subtle (or slower) was seen for NICL5-100, whereas NICL5-50 samples seemed to simply sediment fast. To address it, however, a short-term stability study would have to be performed with several periodic size measurements. NICL5 reproducibility showed to be lower in comparison to NICL10, -20, and -30, hence the increased SEM, most notably on the PDI (**Figure 2** left). Although unimodal and meeting the quality criteria on DLS, the intensity distribution of NICL5 samples was often tailed, even shouldered, towards larger sizes to different extents across replicates.

All formulations were sedimented overnight at 2-8 °C (fridge) but to different extents. The NICL mol% and the extrusion diameter were observed to be inversely proportional to the tendency of sedimentation. Most stable colloidal suspensions were observed for liposomes with higher NICL mol% extruded at smaller membrane cutoff sizes. As expected, the sediment had a larger size and PDI than the visually clear supernatant. Nonetheless, vortexing a sample recovered the initial visual aspect and both size/PDI were similar to a freshly prepared one (**Figure SI 2**).

Overall, having between 20 and 30 NICL mol% was determinant to obtaining acceptable size and PDI. Within this range, however, no clear trend was observed about final TSL size. For 100 nm-extruded CTSLs, the size was practically the same for both NICL20 and NICL30, whilst PDI was notably lower for NICL20-100 (although not significantly different from NICL10-100). As for the samples extruded through 50 nm, size and PDI seem to subtly increase with NICL mol%.

As reasonably expected, NICL mol% directly impacted the CTSLs' ZP. This trend was steep and clear for the samples obtained with 50 nm extrusion filters. For the 100 nm CTSL though, 20 and 30 NICL mol% yielded indistinguishable results (**Figure 2** right). It is in good accordance with the observed colloidal

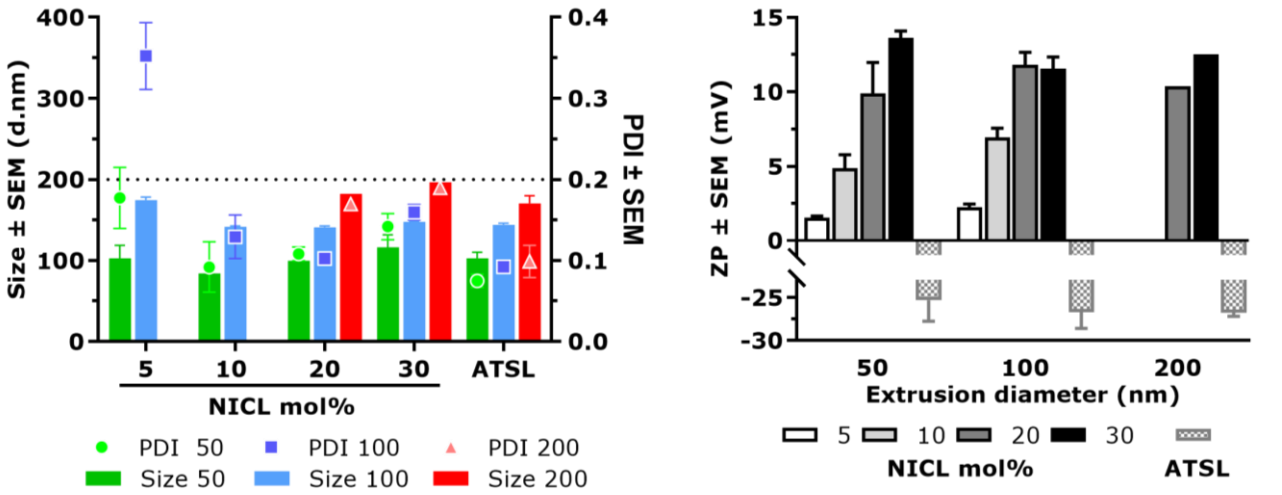


Figure 2. *Characterization of the stable formulations after extrusion by DLS: size (d.nm) and PDI, the dotted line marks size and PDI acceptance thresholds (left); and ZP of CTSL with different NICL mol% (right). With 5 and 10 mol% NICL, 200 nm extrusion did not yield monodisperse For NICL 100 and 50 nm and ATSL, n=3. For NICL 200 nm, n=1.*

stability presented in **Table 1** since the sedimentation was inversely proportional to NICL mol% and extrusion diameter.

None of the CTSLs with mol% NICL > 30 yielded stable formulations. NICL50 films hydrated and extruded well but formed a gel when cooling down to room temperature, which is faster observed in the fridge. NICL75 films hydrate, or disperse, but cannot be extruded since the filter is clogged immediately. NICL100 films hydrated neither with CF 100 mM at pH 7.2 nor HBS at pH 7.4. It was also observed that NICL100 melted below the lipid film drying temperature of 60 °C.

3.2. CF-release from NICL-CTSL is temperature- and time-dependent.

All formulations with 10 and 20 mol% NICL and NICL30-50 exhibited temperature-dependent release (TDR) profiles in biologically relevant media (FCS). It was increasingly less defined and reproducible for higher NICL mol% and larger extrusion diameters, hence the relatively increasing SEM. NICL30-100 and -200 did not show significant temperature sensitiveness (**Figure 3**). The correlation between TSL size and heat-triggered drug release described by Hossann et al was also seen here. Smaller TSLs released higher percentages of CF than larger ones [13].

In general, 50 nm extruded samples released more CF both after 5 and 60 min but also showed higher leakage at low temperatures in FCS. The maximum release after 5 min peaked at 42-43 ºC, with a very subtle trend of the curve shifting towards higher temperatures as NICL mol% increases. Only the 50 nm extruded samples reached over

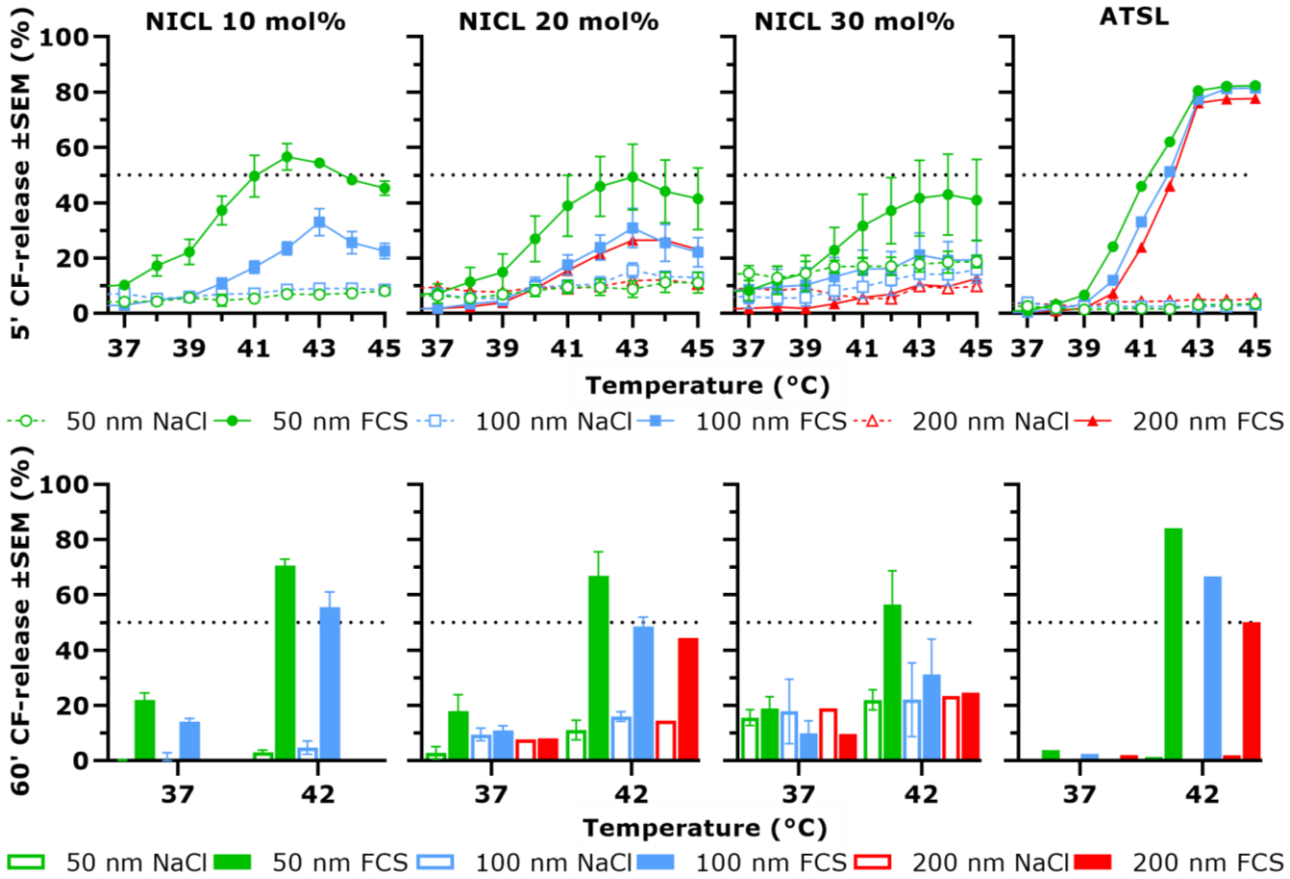


Figure 3. *TDR profiles over 5 min (above) and after 60 min (below) for the most stable formulations pointed with DLS. The dotted line marks 50% CF-release. N=1 for ATSL and NICL 200 nm.*

50% release after 5 min, with NICL10-50 being the most reproducible. Samples extruded through 100 and 200 nm ones yielded similarly worst results in both experiments. On the other hand, the 100 nm sample sets leaked generally less CF than 50 nm ones after 60 min at 37 ºC in FCS. Lastly, the 200 nm extruded samples showed barely any temperature-responsiveness and the relatively highest leakage in all experiments. Therefore, follow-up kinetics experiments focused on 50 and 100 nm extruded CTSLs.

For the same extrusion diameter, ATSL formulations yielded better results than NICL ones in the 5-min experiments. ATSL had the steepest heat-triggered release, peaking at 80% at 43-45 ºC. The leakage was also barely detectable in saline and negligible in FCS in both 5- and 60-min experiments.

The time-dependent release (or release kinetics, RK) results agreed with the ones from TDR. The higher the NICL mol% and the larger the extrusion diameter, the worst the CF-release over 5 minutes. Samples extruded through 50 nm more quickly released their cargo as compared to 100 nm ones. The RK also showed that at the optimal temperature, the steepest increase in CF release was achieved within the first seconds of the experiment (**Figure 4**). It shows that this burst release was also possible with NICL10-50. However, when compared to ATSL [3], the CTSLs here released a lower percentage of their payload in a similar experiment.

As shown by the RK constants (k*), overall, extrusion diameter is related directly proportionally to heat-triggered drug release and inversely proportionally to the CF-leaking. Interestingly, the steepest relative increase of k* was obtained for NICL10-100 (**Figure 4**), which was not straightly obvious from the RK. Still, the SEM was considerably higher, making k* undistinguishable from 41 to 44 °C, precisely covering the range where optimal drug release was pointed out on TDR.

The heat-triggered experiments combined agreed with previously published data by Hossann et al showing that smaller TSLs release their cargo more easily than larger ones. It means more drug delivery [13] but it

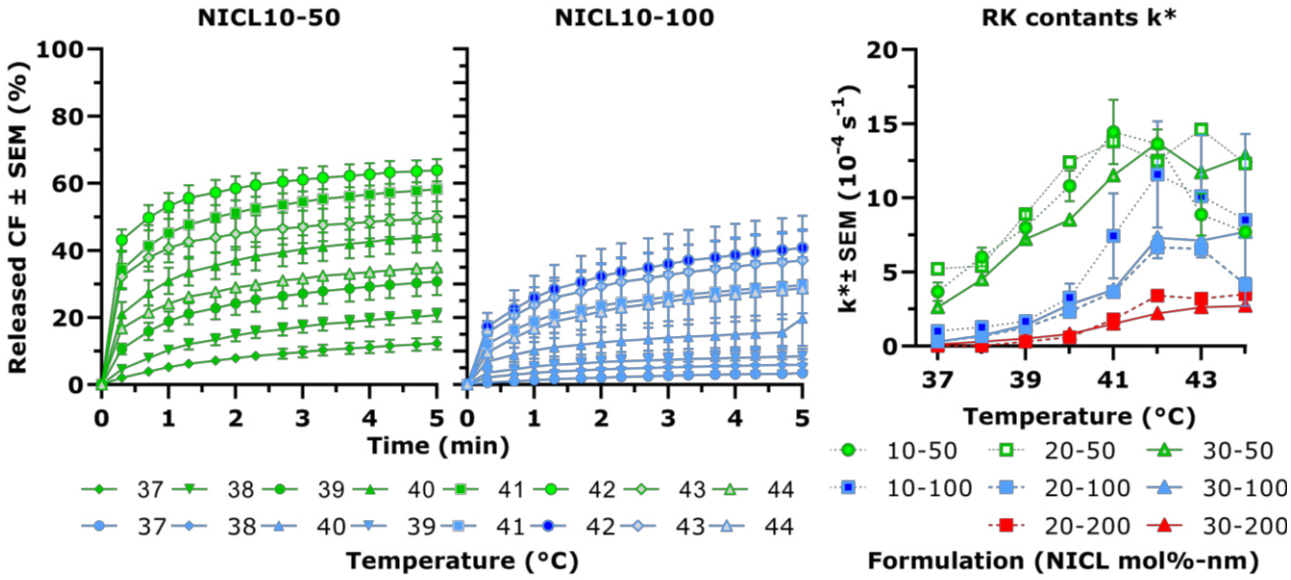


Figure 4. *Time-dependent CF-release from DTSL: RK for the formulations with best TDR (left and middle) and RK constants k* (right) for NICL10-50 and NICL10-100 (n=3) and other DLS stable formulations (n=1 or 2). Maximum release temperatures and best k* profiles are highlighted with bright symbols.*

also implied an increased likelihood of leakage here, which may be attributed to NICL.

3.3. Increasing NICL mol% makes T_m and drug-release less defined.

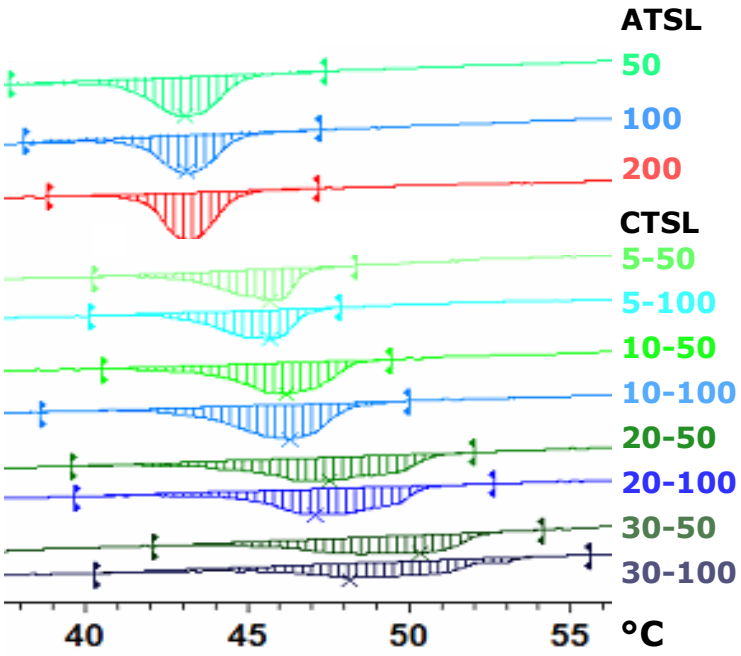
DSC analyses revealed that the higher the NICL mol%, the shallower, wider, and less defined is the T_m of the CTSL. This was in contrast with the sharp T_m of ATSL samples containing 30 mol% of $DPPG_2$. In both cases, however, the extrusion diameter seemed not to notably affect the DSC profile (**Figure 5**). For the CTSLs here, these DSC results were in accordance with their respective time- and temperature-dependent release profiles. For the same TSL formulation, the DSC analyses did not seem to probe the effect of extrusion diameter. Indeed, Biltonen & Lichtenberg showed that T_m is not affected by size for liposomes larger than 70nm [22]. In the same direction, Hossann et al reported similar findings for $DPPG_2$-based ATSL [13].

After failing to hydrate with HBS, NICL100 lipid film was dried and submitted to DSC. The T_m at 52.46 ºC confirms the observation of it having visually melted while drying the lipid film at 60 ºC. Noteworthy, the cooling phase peak at 49.68 °C showed to be sharper, steeper, and better defined than the heating phase one. This 2.48 °C difference was noticeably 4.4-fold higher than the average difference between heating and cooling peaks of 0.56 ± 0.20 °C (**Figure SI. 3**).

While concentrating the samples via centrifugal filtration, it was observed that the filtrate of CTSLs exhibited a faint light green color, indicating the presence of diluted CF. The filtrate from ATSLs, on the other hand, was clear and colorless. Since the centrifugation was done at 4 °C, it is unlikely that the filtrated CF originated from heat-induced release. Hence, the mechanical stress of 14000 rpm could potentially deform the CTSLs up to causing unwanted minor CF leakage.

3.4. In aqueous systems, NICL-CTSLs behave as polyelectrolyte.

Carrasco et al (2021) showed that ionizable cationic lipid nanoparticles behave as polyelectrolytes in solution. Adapting their



	T_m (°C)		
Sample	**Mean**	**SEM**	**n**
ATSL-50	43.35	0.16	3
ATLS-100	43.39	0.14	3
ATSL-200	43.20	0.08	3
NICL5-50	45.52	0.08	3
NICL10-50	45.73	0.24	3
NICL20-50	47.23	0.31	2
NICL30-50	48.67	1.70	2
NICL5-100	45.38	0.33	2
NICL10-100	46.32	0.53	3
NICL20-100	47.01	0.10	2
NICL30-100	48.18	-	1

Figure 5. *DSC curves (left) and tabled T_m of the most stable formulations (right) on DLS.*

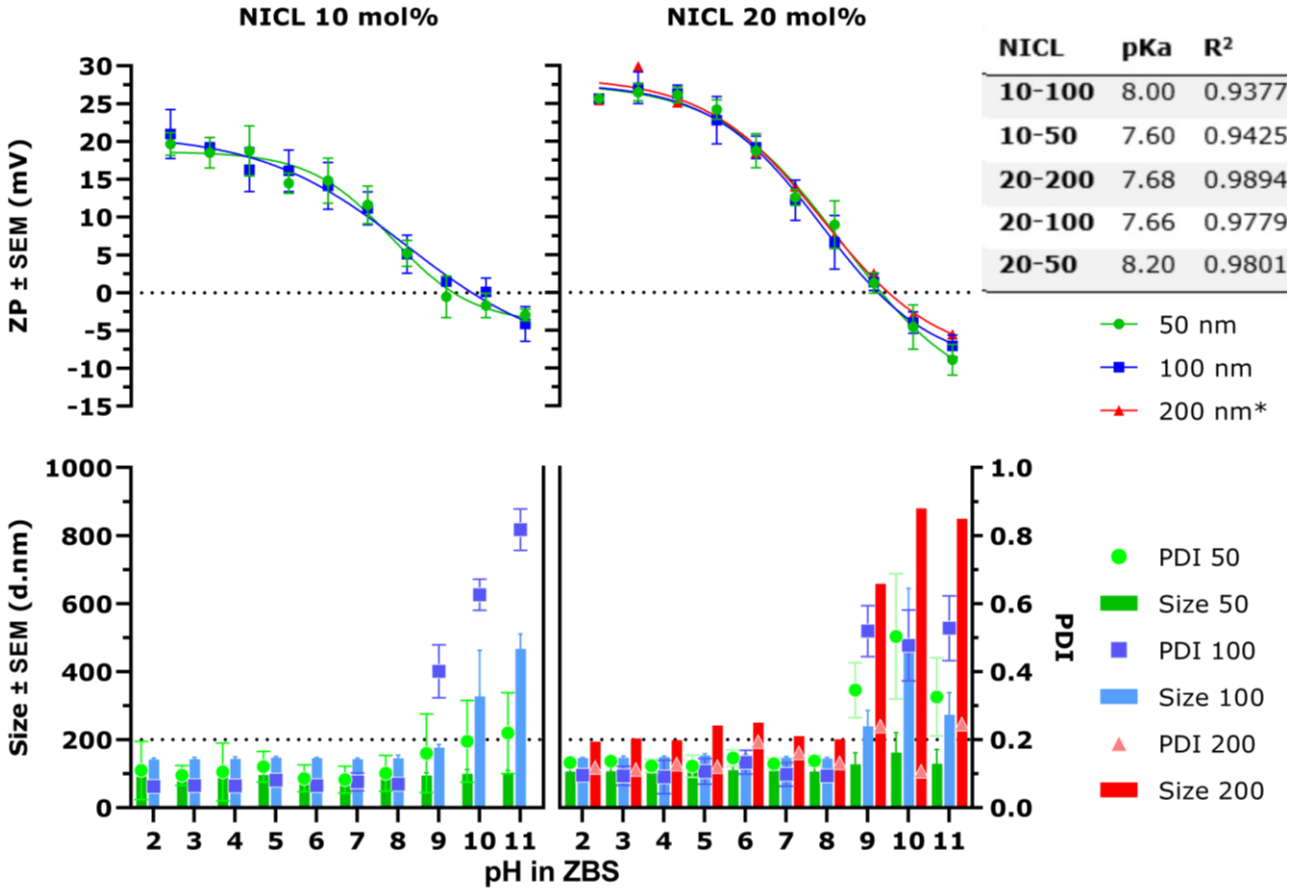
approach to NICL-CTSLs here, a similar behavior was observed [21]. The ZP of CTSLs decreased with increasing pH while the size and the PDI remain stable up until reached their isoelectric point (pI) around pH 9-10. Since the net charge of the nanoparticle's surface at this point is expected to be 0, they started to aggregate. This was noted by the increase in size and, more steeply, PDI observed at and above the pI (**Figure 6**).

Again, the trend with extrusion diameter was spotted. The increase in size for 50 nm-extruded particles was much more subtle than for the 100 nm ones. The PDI was affected more intensely, but again, NICL 100 nm ones to a much lesser extent than the latter. However, the SEM of the PDI was widened more for samples extruded through 50 nm than through 100 nm (**Figure 6** bottom).

DLS results agreed with visual observations. Sample dilutions from pH 2 to 8 were clear, while from pH 9 to 11 the systems became instantly turbid upon dilution. As expected, CTSLs and ATSLs answered to pH changes in opposite fashions (**Figure SI 5**).

Interestingly, a subtle increase of SEM in the PDI is observed for NICL10-50 at lower pHs. It might be related to lipid hydrolysis and the formation of small micelles and/or larger aggregate. Oxidation, on the other hand, is less likely since the lipids used here have saturated alkyl chains and the temperature was mild (RT) [23]. One way to check the hydrolysis hypothesis is by looking for the lysolipid and fatty acid pairs in a sample analyzed by HPLC-CAD at different pHs.

When observing individual DLS results at pH ≥ 9, the formation of both smaller and



NICL	pKa	R^2
10-100	8.00	0.9377
10-50	7.60	0.9425
20-200	7.68	0.9894
20-100	7.66	0.9779
20-50	8.20	0.9801

Figure 6. *Effect of pH on ZP (above) and size (below) for NICL10-50 and NICL10-100. Fitting the ZP values to the eHH yielded the pKa values and respective R^2 on the table (upper right). *n=1 for 200 nm.*

larger populations of particles was observed, at the spent of reducing the population around 100 nm (**Figure SI 4**). On one hand, it could be a sign that the mechanism of size increasing is coalescence. On the other hand, it could be that some lipids are hydrolyzing and there was a formation – transiently or not – of lysolipid and/or fatty acids micelles.

ZP values were fitted to the eHH, with the mid-height between upper and lower Y-plateaus graphically representing CTSL's pKa. These varied from 7.60 to 8.20 depending both on NICL mol% and extrusion diameter. The correlation coefficient R^2 was larger than 0.9 for all the curves supporting the consideration of the obtained pKa values. Comparing the two plots, one can see that the higher NICL mol% yielded a wider yet more clearly defined titration curve (**Figure 6 top**).

3.5. NICL-CTSL bind to tumor cells *in vitro* better than ATSL.

As illustrated in **Figure 7**, NBD-labelled CTSLs (green) are localized mainly on the tumor cell surfaces. The intensity of the signal correlated with NICL mol%, confirming the assumption that CTSLs with higher ZP would

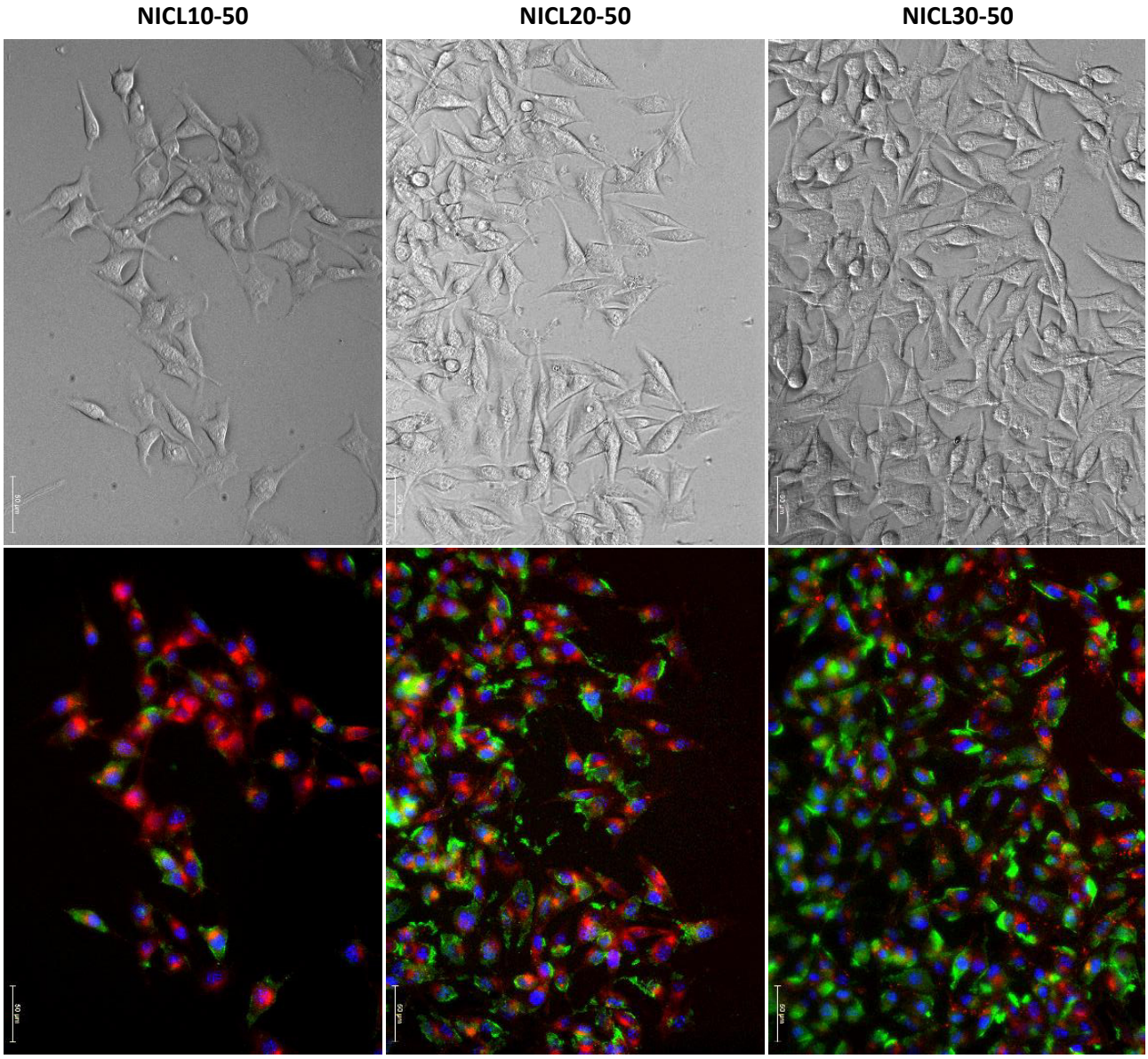


Figure 7. *Live cell fluorescence microscopy bright field (top) and RGB merged pictures (bottom) for B16 cells treated with different unloaded NBD-labelled CTSL formulations. Scale bar = 50 µm.*

bind more intensely to the negatively charged surface of tumor cells. Lysotracker (red) stains acidic organelles, chiefly lysosomes. Orange appears upon red and green overlay, which can be interpreted as internalization of the labeled nanoparticles. This was seldom spotted on all the three CTSLs, but relatively more noticeable for cells treated with NICL20-50. Co-localization with the Höchst-stained (blue) nuclei was observed in none of the cases. This was expected since liposomes may disassemble when internalized (e.g., by lysosomal activity) or fused with the cell membrane.

The observations and comments so far are in accordance with the controls shown in **Figure 8**. To assess the effect of surface charge, neutral, TSLs extruded at 50 nm (0TSL-50) were prepared using DPPC/DSPC with an 8:2 molar ratio. Due to a ZP close to 0 mV, there is not enough electrostatic repulsion between particles, so they tend to aggregate. It is expected that larger particles sedimented quickly and mechanically deposited on top of the cells or the surface of the

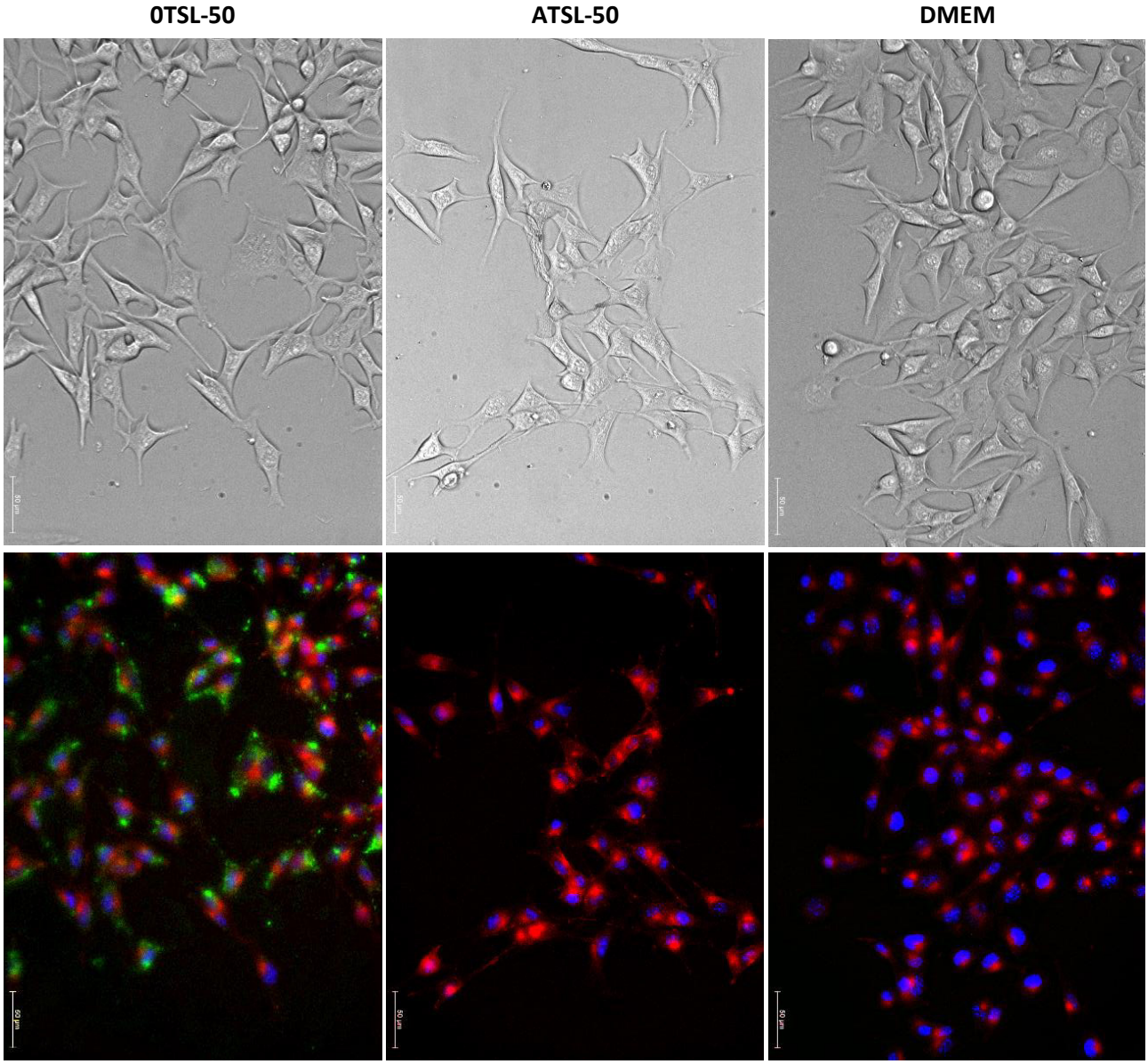


Figure 8. *Live cell fluorescence microscopy bright field (top) and RGB merged pictures (bottom) for B16 cells treated with different unloaded NBD-labelled TSLs or DMEM (control). Scale bar = 50 µm.*

slide. The latter could be responsible for the observed dotted pattern.

ATSLs here were expected to interact less intensely with the negatively charged cancer cell surfaces, hence the absence of green in this control. The ATSLs have mostly been washed away during the staining procedure. It is in good agreement with a previous experiment by Petrini et al, who showed that $DPPG_2$-based CTSLs live targets tumor and endothelial cells more than $DPPG_2$-based ATSLs [5]. The shorter time of incubation here (30 min against 60) and the different cell lines (B16 against B175 and HUVEC) could potentially explain the ATSL control.

Experiments with cells incubated with non-containing liposomes cell culture media promoted no visible NBD signal (green), as expected. Comparing **Figures 7** and **8**, one can see that CTSLs promoted better adherence to tumor cell membranes than ATSLs. Being much less retained made the signal very weak for the latter, getting barely noticeable in the merged picture.

4. Discussion

CF has been used to study the payload release from TSLs since the pioneering work by Yatvin [12]. Its convenient physicochemical properties, particularly its fluorescence, make it an overall good drug model [24]. At high concentrations, it is dark red and barely fluorescent in an aqueous solution due to self-quenching. Upon dilution, which happens during CF-release, it is bright green and highly fluorescent [19,24].

Here, the 100 mM CF pH 7.2 was observed as a dark red clear solution. Upon dispersion of the lipid film, it turned into a milky dark red suspension visually resembling blood. After purified by SEC, the liposome suspensions had a homogenously turbid orange look, like orange juice. CF was self-quenched up to here. After incubating the liposomes with Triton, a clear bright green solution was formed due to CF dequenching upon dilution.

It is interesting to point out that despite having suboptimal DLS characteristics, the 5 min TDR of the 5 mol% NICL samples was very similar to the 10 mol% ones (**Figure 3**). The DSC results in **Figure 5** indeed showed that NICL5 has a better-defined T_m, which correlates with the steeper and higher CF-release on TDR. However, considering that DLS results suggest that these formulations are prone to aggregation, it might simply be a feature of larger vesicles.

Mouritsen (2011) reviewed the concept of curvature in lipid assemblies in the context of drug delivery and nanomedicine. Lipids differ from the other biomacromolecules (carbohydrates, proteins, and nucleic acids) for not being polymers in natural conditions. Concerning vesicles like liposomes, the intrinsic curvature stress of the membrane and its tendency to form curved shapes implies entropic instability. In fact, the lateral stress- or pressure profile of liposomes contributes to the explanation of the drug release mechanism. The association of proteins to the lipid membrane surface also modulates its physicochemical behavior [25]. Here, it was shown that proteins from FCS are crucial for the thermal-induced CF-release. The thermal experiments altogether suggest that smaller TSLs are more prone to release their payload. This feature is enhanced upon heat stimulus for bringing the system to a less stable state at the T_m. It potentially relates to the relative

surface curvature, which is inversely proportional to the particle radius. This was already observed for ATSLs in previous studies [13] and it can be seen in **Figure 2** here.

Baptista et al showed that CF-loaded soy lecithin liposomes are sensitive to external pH. They found that the dye release to be much faster in acidic than in basic conditions [26]. The zeta-titration experiments suggested that the PDI increase in acidic pHs could be related to a change in the distribution of size populations, meaning that CF could eventually be released during reassembling of the TSLs (**Figure 6**). Notwithstanding, it could also mean drug delivery in a therapeutic scenario since the liposome would still release their payload in an acidic tumor environment – especially if internalized into lysosomes.

The lipid nanoparticles (LNP) developed by Carrasco et al are designed to be taken up by endocytosis and fuse with lysosomal membranes to release their payload intracellularly, similarly to the COVID-19 mRNA vaccines. Thus, the target pKa for their LNPs is between 6 and 7 in the anionic fluorescent dye 2-(p-toluidino)-6-naphthalenesulfonic acid (TNS) binding assay, which is ~0.7 units lower than the ZP one. Their pIs ranged from 5.4 to 6.6 [21]. From **Figure 6** one can see that the NICL-based CTSLs had higher pKa values (7.6 to 8.2) and pI (~9.0), which can be appropriate for intravascular heat-triggered drug release. The CTSLs here have higher ZP at physiological pH, as shown in **Figure 2**. This could be forecasted as better stability in circulation, up until it reaches the mild HT zone, which is demonstrated in **Figure 3**. Then, according to **Figure 4**, the burst release is achieved within seconds. Clearly, further *in vivo* experiments are needed to confirm the assumptions derived from these initial observations.

The live-cell fluorescence microscopy results agreed with previous reports on CTSLs [5,18,20]. The higher the NICL mol% the higher the biding, as expected. Bleaching, however, showed to be a serious issue during image acquisition. And it is more significant for the formulations that interacted the less. Hence, quantitative conclusions cannot be drawn, but the main trend was spotted.

Considering all the results together, the formulation with 10 mol% NICL extruded through 50 nm exhibited the best features after the characterization. Short-term stability studies would be the next step to follow up with this formulation.

5. Conclusions and Perspectives

Here it is shown that NICL can successfully be used to manufacture CF-loaded CTSL. The results showed that the extrusion pore filter size and NICL mol% are critical process parameters. The former mostly affects colloidal stability and release-ability, while the latter also directly impacts CTSLs surface charge (ZP, hence colloidal stability), temperature- and time-dependent release profiles, T_m, and pKa. Results also strongly point out the interplay between the two parameters.

The pKa of NICL-based CTSL ranged from 7 to 8 depending on NICL mol% and overall did not seem to be affected by extrusion size. Further *in vitro* studies including a TNS-binding assay are on the outlook to improve the understanding of the pH-responsiveness of these novel CTSLs.

Live-cell fluorescence microscopy showed the ability of NICL-based CTSLs to bind to

negatively charged B16 melanoma cells. It agrees with previous reports and raises the hypothesis that these formulations could increase the retention of the formulation in tumor sites, which possibly can contribute to increasing local drug delivery.

Amongst the investigated formulations, the one with 10 mol% NICL extruded through 50 nm showed the best compromise between colloidal stability, liposomal yield, EE, release-ability, and temperature- and pH-responsiveness. Next, quantitative cell-binding experiments such as FACS and *in vivo* testing of dye delivery would follow up.

6. Acknowledgments

Vladyslav Nikitchenko and Lisa Pointner, Thermosome GmbH, DE, and Angela Knauerhase, Bettina Heiß, Sinan Emre Güler, and Xi Zhu, LMU Klinikum, DE, for the daily support in the research. The Federal ministry of education and research (BMBF) 031B0759B for funding the research and the NANOMED EMJMD for providing TVM's scholarship.

7. References

[1] Kneidl B, Peller M, Winter G, Lindner LH, Hossann M. Thermosensitive liposomal drug delivery systems: state of the art review. Int J Nanomedicine 2014;9:4387–98. https://doi.org/10.2147/IJN.S49297.

[2] Kinam Park. Drug Delivery: Fundamentals and Applications. vol. 1. 2nd edition. Boca Raton, FL, USA: CRC Press; 2016.

[3] Hossann M, Hirschberger J, Schmidt R, Baumgartner C, Zimmermann K, Baer S, et al. A Heat-Activated Drug-Delivery Platform Based on Phosphatidyl-(oligo)-glycerol Nanocarrier for Effective Cancer Treatment. Advanced NanoBiomed Research 2021;1:2000089. https://doi.org/10.1002/anbr.202000089.

[4] Lokerse WJM, Lazarian A, Kleinhempel A, Petrini M, Schwarz P, Hossann M, et al. Mechanistic investigation of thermosensitive liposome immunogenicity and understanding the drivers for circulation half-life: A polyethylene glycol versus 1,2-dipalmitoyl-sn-glycero-3-phosphodiglycerol study. Journal of Controlled Release 2021;333:1–15. https://doi.org/10.1016/j.jconrel.2021.03.014.

[5] Petrini M, Lokerse WJM, Mach A, Hossann M, Merkel OM, Lindner LH. Effects of Surface Charge, PEGylation and Functionalization with Dipalmitoylphosphatidyldiglycerol on Liposome-Cell Interactions and Local Drug Delivery to Solid Tumors via Thermosensitive Liposomes. Int J Nanomedicine 2021;16:4045–61. https://doi.org/10.2147/IJN.S305106.

[6] McDonald DM. Uptake of Cationic Liposomes by Normal and Angiogenic Endothelial Cells In Vivo. Nature Biotechnology 1999;17:14–14. https://doi.org/10.1038/70129.

[7] van Valenberg FJP, Brummelhuis IS, Lindner LH, Kuhnle F, Wedmann B, Schweizer P, et al. DPPG2-Based Thermosensitive Liposomes with Encapsulated Doxorubicin Combined with Hyperthermia Lead to Higher Doxorubicin Concentrations in the Bladder Compared to Conventional Application in Pigs: A Rationale for the Treatment of Muscle-Invasive Bladder Cancer. International Journal of Nanomedicine 2021;Volume 16:75–88. https://doi.org/10.2147/IJN.S280034.

[8] Liu P, Chen G, Zhang J. A Review of Liposomes as a Drug Delivery System: Current Status of Approved Products, Regulatory Environments, and Future Perspectives. Molecules 2022;27. https://doi.org/10.3390/molecules27041372.

[9] Kozma GT, Shimizu T, Ishida T, Szebeni J. Anti-PEG antibodies: Properties, formation, testing and role in adverse immune reactions to PEGylated nanobiopharmaceuticals. Advanced Drug Delivery Reviews 2020;154–155:163–75.

https://doi.org/10.1016/j.addr.2020.07.024.

[10] Mohamed M, Abu Lila AS, Shimizu T, Alaaeldin E, Hussein A, Sarhan HA, et al. PEGylated liposomes: immunological responses. Science and Technology of Advanced Materials 2019;20:710–24. https://doi.org/10.1080/14686996.2019.1627174.

[11] Prabhakar U, Maeda H, Jain RK, Sevick-Muraca EM, Zamboni W, Farokhzad OC, et al. Challenges and Key Considerations of the Enhanced Permeability and Retention Effect for Nanomedicine Drug Delivery in Oncology. Cancer Research 2013;73:2412–7. https://doi.org/10.1158/0008-5472.CAN-12-4561.

[12] Yatvin MB, Weinstein JN, Dennis WH, Blumenthal R. Design of Liposomes for Enhanced Local Release of Drugs by Hyperthermia. Science (1979) 1978;202:1290–3. https://doi.org/10.1126/science.364652.

[13] Hossann M, Wang T, Wiggenhorn M, Schmidt R, Zengerle A, Winter G, et al. Size of thermosensitive liposomes influences content release. Journal of Controlled Release 2010;147:436–43. https://doi.org/10.1016/j.jconrel.2010.08.013.

[14] Regenold M, Bannigan P, Evans JC, Waspe A, Temple MJ, Allen C. Turning down the heat: The case for mild hyperthermia and thermosensitive liposomes. Nanomedicine: Nanotechnology, Biology, and Medicine 2022;40. https://doi.org/10.1016/j.nano.2021.102484.

[15] Needham D, Anyarambhatla G, Kong G, Dewhirst MW. A new temperature-sensitive liposome for use with mild hyperthermia: characterization and testing in a human tumor xenograft model. Cancer Res 2000;60:1197–201.

[16] Sebeke LC, Castillo Gómez JD, Heijman E, Rademann P, Simon AC, Ekdawi S, et al. Hyperthermia-induced doxorubicin delivery from thermosensitive liposomes via MR-HIFU in a pig model. Journal of Controlled Release 2022;343:798–812. https://doi.org/10.1016/j.jconrel.2022.02.003.

[17] Thermosome GmbH. Thermosome – intravascular drug release 2022. https://www.thermosome.com/ (accessed June 21, 2022).

[18] Dicheva BM, ten Hagen TLM, Schipper D, Seynhaeve ALB, van Rhoon GC, Eggermont AMM, et al. Targeted and heat-triggered doxorubicin delivery to tumors by dual targeted cationic thermosensitive liposomes. Journal of Controlled Release 2014;195:37–48. https://doi.org/10.1016/j.jconrel.2014.07.058.

[19] Kneidl BC. Formulation studies, lyophilization and in vivo investigation of 1,2-dipalmitoyl-sn-glycero-3-phosphodiglycerol-based thermosensitive

liposomes for the delivery of gemcitabine, irinotecan and SN-38. Doctoral Thesis. Ludwig-Maximilians-Universität München, 2017. https://doi.org/10.5282/edoc.25415.

[20] Matteo Petrini. Cationic and anionic phosphatidyldiglicerol-based thermosensitive liposomes for the targeted delivery of chemotherapeutics and immunoadjuvants. Doctoral Thesis. Ludwig-Maximilians-Universität München, 2019.

[21] Carrasco MJ, Alishetty S, Alameh MG, Said H, Wright L, Paige M, et al. Ionization and structural properties of mRNA lipid nanoparticles influence expression in intramuscular and intravascular administration. Communications Biology 2021;4. https://doi.org/10.1038/s42003-021-02441-2.

[22] Biltonen RL, Lichtenberg D. The use of differential scanning calorimetry as a tool to characterize liposome preparations. vol. 64. 1993.

[23] Grit M, Crommelin DJA. Chemical stability of liposomes: implications for their physical stability. Chemistry and Physics of Lipids 1993;64:3–18. https://doi.org/10.1016/0009-3084(93)90053-6.

[24] le Guern F, Mussard V, Gaucher A, Rottman M, Prim D. Fluorescein derivatives as fluorescent probes for ph monitoring along recent biological applications. International Journal of Molecular Sciences 2020;21:1–23. https://doi.org/10.3390/ijms21239217.

[25] Mouritsen OG. Lipids, curvature, and nanomedicine. European Journal of Lipid Science and Technology 2011;113:1174–87. https://doi.org/10.1002/ejlt.201100050.

[26] Baptista ALF, Coutinho PJG, Oliveira MECDR, Gomes JINR. Effect of pH on the Control Release of Microencapsulated Dye in Lecithin Liposomes. II. Journal of Liposome Research 2003;13:123–30. https://doi.org/10.1081/LPR-120020315.

8. Supplementary Information

The lipid content deviated slightly from the nominal values in the planned formulations (**Figure SI 1**), but still in acceptable ranges. For NICL5 samples, the standard absence and the low CAD signal combined could explain NICL overestimation. $DPPG_2$ values were consistent and reproducible, besides being more precisely determined due to standard availability.

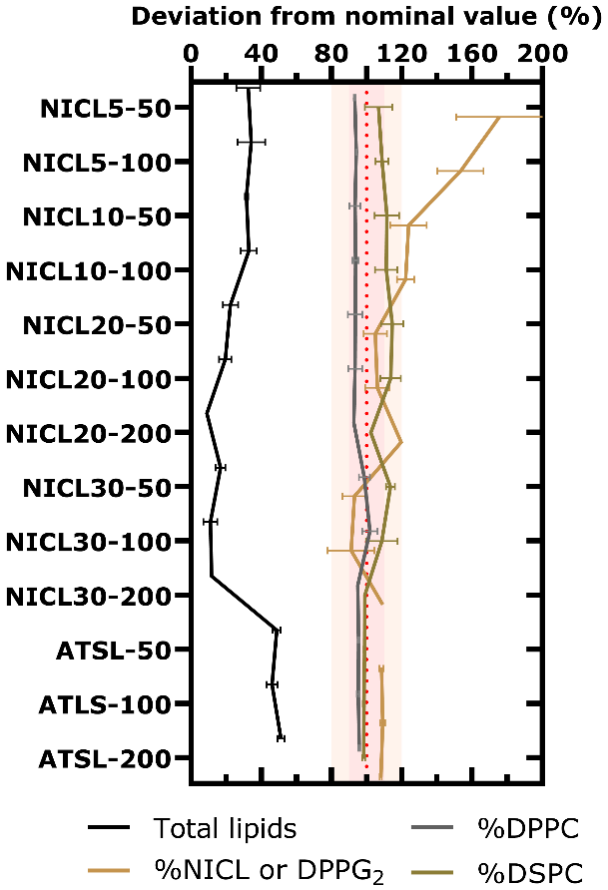
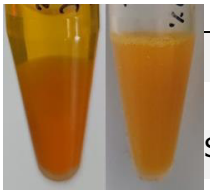


Figure SI 1. *Deviation from nominal values in the lipid composition for the stable formulations after extrusion. The red dotted line marks the 100% referential. The red and orange shaded areas represent ± 10 and 20% respectively.*

Despite sedimenting, vortexing recovers the fresh aspect of the formulations. As a representative example in **Figure SI 2**, pictures of a NICL10-50 before and after vortexing and relevant DLS data are shown. Notice the dark orange sediment at the bottom and the light clear bright orange supernatant at the top turning back into the homogenous milky orange suspension. The size distribution by intensity of a NICL10-100 sample is also shown (**Figure SI 2**).



Sample	Size (nm)	PDI
Fresh	82.90	0.146
Sediment	107.4	0.194
Supernatant	64.53	0.053
Vortexed	84.35	0.174

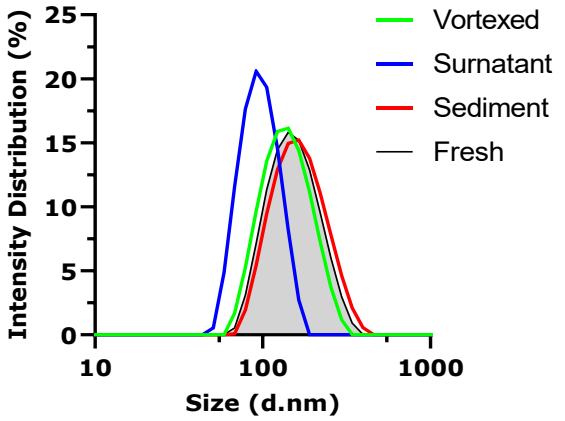


Figure SI 2. *Visual aspect of a NICL10-50 stored overnight at 4 °C (upper left) and after being shortly vortexed (upper middle) and Size and PDI values for the sediment, supernatant, and vortexed sample, compared to the fresh one (upper right). Size distribution by intensity of a fresh NICL10-100, its sediment, its supernatant, and after vortexing it (bottom).*

The peak temperature between heating and cooling events on DSC was noticeably different for NICL100. At the same time, the profile is clear and narrow (**Figure SI 3**).

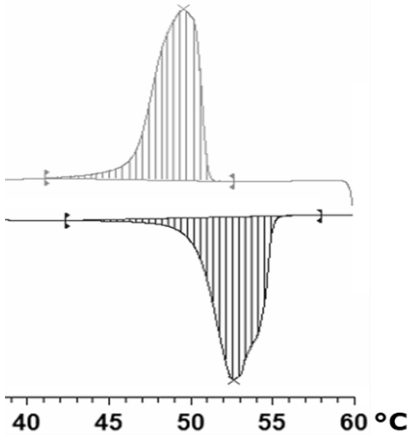


Figure SI 3. *Heating (above) and cooling (below) phases of the thermogram for NICL-100 on DSC.*

The DLS results suggest that the CTSLs coalesce at high pH values, as there is the simultaneous formation of populations with larger and smaller sizes (**Figure SI 4**). Stressing that the distribution is by intensity, larger populations might be overestimated.

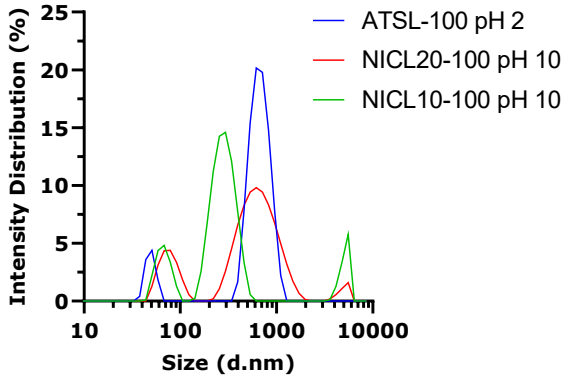


Figure SI 4. *Formation of smaller and larger peaks on DLS for different NICL10-100 sample at pH 10 and 11, suggesting coalescence as the mechanism of particle size increase.*

ATSL pKa could not be determined by zeta-titration because it is beyond the range of the buffers (**Figure SI 5**).

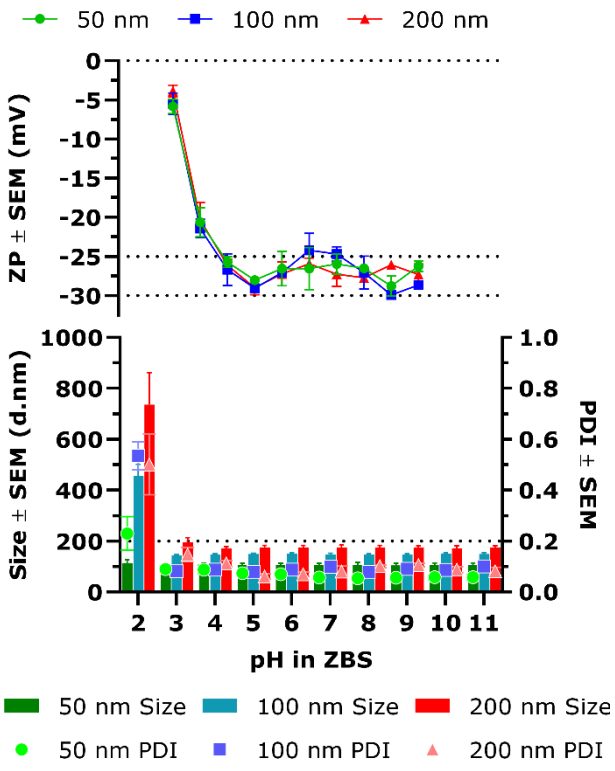


Figure SI 5. *ZP (above), Size, and PDI (below) of ATSLs during zeta-titration.*

The upper plateau could not be probed. Nonetheless, an opposite behavior as compared to CTSLs was observed. Its ZP oscillates between -25 and -30 mV from pH 11 down to pH 4. At pH 3, it starts to increase above this range while clear aggregation is observed at pH 2 only.